Received: 14 September 2021 | Revised: 25 June 2022 | Accepted: 8 July 2022

DOI: 10.1002/jnm.3049

SPECIAL ISSUE PAPER

WILEY

A comparative study on electromagnetic quasistatic time-domain field calculations

Marvin-Lucas Henkel[1] | **Fotios Kasolis**[1] | **Sebastian Schöps**[2] | **Markus Clemens**[1]

[1]Chair of Electromagnetic Theory, University of Wuppertal, Wuppertal, Germany

[2]Computational Electromagnetics Group, Technical University of Darmstadt, Darmstadt, Germany

Correspondence
Marvin-Lucas Henkel, Chair of Electromagnetic Theory, University of Wuppertal, Rainer-Gruenter-Strasse 21, 42119 Wuppertal, Germany.
Email: mhenkel@uni-wuppertal.de

Funding information
Deutsche Forschungsgemeinschaft, Grant/Award Number: CL143/11-2 CL143/18-1

Abstract

Electromagnetic quasistatic field models, which take into consideration resistive, inductive, and capacitive effects, have been introduced for electrical engineering applications whose geometrical characteristics, combined with the operational frequencies, suggest negligible radiation phenomena. Here, a monolithic variant of a previously proposed two-step electromagnetic quasistatic algorithm and a two-step time-domain Maxwell formulation are presented, together with relevant initial-boundary value problems. In view of numerical experiments, the fields that are obtained with the two-step electromagnetic quasistatic algorithm, its monolithic variant, and the two-step time-domain Maxwell formulation are compared and turn out to be in good agreement.

KEYWORDS

electromagnetic fields, finite element method, quasistatic fields, time-domain analysis, two-step time-domain Maxwell

1 | INTRODUCTION

In electrical engineering applications, such as resonant coils, inductive charging systems, and high-voltage insulators, it is often assumed that the rate of change of either the magnetic flux density $\boldsymbol{B}$ or that of the electric flux density $\boldsymbol{D}$ is vanishing. Under any of these assumptions, the fields are said to be quasistatic, with the resulting fields being called electro-quasistatic (EQS) and magneto-quasistatic (MQS) for $\partial_t \boldsymbol{B} = \partial \boldsymbol{B}/\partial t = \boldsymbol{0}$ and $\partial_t \boldsymbol{D} = \boldsymbol{0}$, respectively. More recently, the interest of the engineering community has been shifted toward electromagnetic quasistatic (EMQS) field models,[1–7] that is, models that are able to capture all effects—resistive, inductive, and capacitive—excluding radiation, such as for instance the two-step Darwin model.[8] This two-step approach is based on the observation that MQS fields can be gauged by first solving an EQS problem and then employing the resulting EQS current as a source term for the equation that governs the MQS field. More precisely, let the EQS current be

$$\mathbf{J}_{\mathrm{EQS}} = -\varepsilon \nabla \partial_t \varphi - \sigma \nabla \varphi, \tag{1}$$

where φ is the sought scalar EQS potential, $\varepsilon > 0$ is the electric permittivity, and $\sigma \geq 0$ is the electric conductivity. Then, in the absence of external currents, the EQS problem $\nabla \cdot \boldsymbol{J}_{\mathrm{EQS}} = 0$ is solved for φ, while the resulting current $\boldsymbol{J}_{\mathrm{EQS}}$ appears in the MQS equation.

$$\nabla \times \mu^{-1} \nabla \times \mathbf{A} + \sigma \partial_t \mathbf{A} = \mathbf{J}_{\mathrm{EQS}} \tag{2}$$

as a known term. By taking the divergence of (2), it immediately follows that the vectorial MQS potential $\boldsymbol{A}$ satisfies the condition.

$$\nabla \cdot \sigma \partial_t \mathbf{A} = 0. \tag{3}$$

Provided that the computational domain Ω constitutes of a non-conductive subdomain Ω_{V} with $\sigma|\Omega_{\mathrm{V}} = 0$ and a conductive subdomain whose conductivity $\sigma|\Omega_{\mathrm{C}} > 0$ is constant, Equation (3) provides a partial gauging in the conductive regions only, that is, $\nabla \cdot \partial_t \boldsymbol{A}|\Omega_{\mathrm{C}} = 0$. Although this partial gauging is sufficient for computing the magnetic flux density $\boldsymbol{B} = \nabla \times \boldsymbol{A}$, the electric field intensity needs to be corrected by the rate of change of the vectorial MQS potential, that is,

$$\mathbf{E} = -\nabla \varphi - \partial_t \mathbf{A}, \tag{4}$$

and hence, the vectorial MQS potential needs to be well-determined everywhere in the computational domain.

The rest of the paper is organized as follows. In the forthcoming section, the continuous initial-boundary value problems of interest are introduced, in a general setting, and suitable discrete formulations are presented. The section concludes with two algorithms for computing EMQS fields; one algorithm for the two-step approach and one for the monolithic variant. In the next section, both the two-step algorithm and its monolithic variant are numerically validated against each other and against the time-domain two-step Maxwell scheme. The last section concludes the paper.

2 | PROBLEM STATEMENT

Suppose that the device of interest is contained in a bounded and simply connected domain $\Omega \subset \mathbb{R}^3$ whose boundary $\partial\Omega$ is Lipschitz, such as those depicted in Figure 1. The domain Ω is free from charge and current sources, while it constitutes of two disjoint domains Ω_{V} and Ω_{C}, which are occupied by void and conductive material, respectively. A third disjoint subdomain Ω_{D} that is occupied by dielectric material with vanishing conductivity may be present, as for

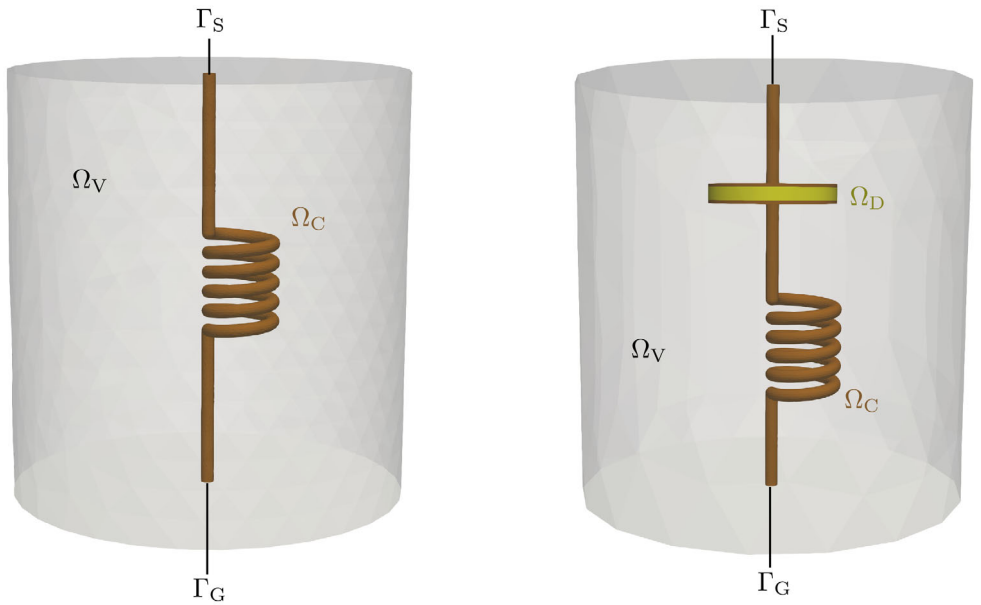

FIGURE 1 Devices that exhibit resistive, capacitive, and inductive phenomena, and are suitable for testing electromagnetic quasistatic formulations

instance the RLC circuit[9] consisting of a resistor (R), an inductor (L), and a capacitor (C), depicted on the most-right side of Figure 1. All subdomains of Ω are also assumed to have Lipschitz interfaces. The terminals of the device reach the boundary $\partial\Omega$ at the surfaces Γ_E and Γ_G, with Γ_E supplying a time-dependent excitation voltage.

$$\varphi \,|\, \Gamma_E = \varphi_E(t) = \varphi_{\max} \cdot \min(ft, 1) \cdot \sin(2\pi ft) \tag{5}$$

and Γ_G set to ground, that is, $\varphi|\Gamma_G = 0$. The rest of the boundary of Ω is assumed to be electrically insulating, and hence, a vanishing Neumann boundary condition is imposed on $\partial\Omega \setminus (\Gamma_E \cup \Gamma_G)$ for the scalar EQS potential. Furthermore, the tangential component of the vectorial MQS potential is assumed to be vanishing on $\partial\Omega$, that is, $\boldsymbol{n} \times \boldsymbol{A}|\partial\Omega = \mathbf{0}$, where $\boldsymbol{n}$ is the outward pointing unit normal on $\partial\Omega$. Then, for all $t \in I = [0, T]$ with $T > 0$, the scalar EQS potential φ satisfies the initial-boundary value problem.

$$\begin{aligned} &\nabla \cdot (\sigma \nabla \varphi + \varepsilon \nabla \partial_t \varphi) = 0 \text{ in } \Omega \times I, \quad \varphi|\{t = 0\} = 0, \quad \varphi|\Gamma_G \times I = 0, \\ &\varphi|\Gamma_E \times I = \varphi_E(t), \quad \partial\varphi/\partial n|\partial\Omega, \quad (\Gamma_E \cup \Gamma_G) \times I = 0 \end{aligned} \tag{6}$$

while, provided the solution of problem (6), the vectorial MQS potential $\boldsymbol{A}$ is obtained by solving the initial-boundary value problem.

$$\nabla \times \mu^{-1} \nabla \times \mathbf{A} + \sigma \partial_t \mathbf{A} = \mathbf{J}_{\text{EQS}} \text{ in } \Omega \times I, \quad \mathbf{A} \,|\, \{t = 0\} = \mathbf{0}, \quad \mathbf{n} \times \mathbf{A} \,|\, \partial\Omega \times I = \mathbf{0}. \tag{7}$$

To state the variational forms that are associated with problems (6) and (7), consider the standard Sobolev spaces $H(\text{grad}, \Omega) = H^1(\Omega)$, $H(\text{curl}, \Omega)$ and define

$$H_a(\text{grad}, \Omega) = \{\psi \in H(\text{grad}, \Omega) : \psi|\Gamma_E = a, \psi|\Gamma_G = 0\}, \quad H_0(\text{curl}, \Omega) = \{\mathbf{w} \in H(\text{curl}, \Omega) : \mathbf{n} \times \mathbf{w}|\partial\Omega = \mathbf{0}\}. \tag{8}$$

Then, problems (6) and (7) imply the following variational problems.

$$\text{find } \varphi \in H_{\varphi(t)}(\text{grad}, \Omega) \text{ such that } \int_\Omega \sigma \nabla\psi \cdot \nabla\varphi \, d\Omega + \int_\Omega \varepsilon \nabla\psi \cdot \nabla \partial_t \varphi \, d\Omega = 0 \quad \forall \psi \in H_0(\text{grad}, \Omega), \tag{9}$$

$$\begin{aligned} \text{find } \mathbf{A} \in H_0(\text{curl}, \Omega) \text{ such that } &\int_\Omega \mu^{-1} \nabla \times \mathbf{w} \cdot \nabla \times \mathbf{A} \, d\Omega + \int_\Omega \sigma \mathbf{w} \cdot \partial_t \mathbf{A} \, d\Omega \\ &= \int_\Omega \mathbf{w} \cdot \mathbf{J}_{\text{EQS}} \, d\Omega \quad \forall \mathbf{w} \in H_0(\text{curl}, \Omega). \end{aligned} \tag{10}$$

Given that both problems (9) and (10) can be stiff, the trapezoidal rule, which is second-order accurate and A-stable, is used for time-discretization. To this end, consider a partition $(t_0, t_1), (t_1, t_2), \ldots, (t_{N-1}, t_N)$ of the time interval I, with $t_0 = 0$, $t_N = T$, and timestep $\Delta t = t_{n+1} - t_n$ for all $n \in \{0, 1, \ldots, N-1\}$. Then, the trapezoidal rule results in the time-discrete equations.

$$\int_\Omega \left(\frac{2\varepsilon}{\Delta t} + \sigma \right) \nabla\psi \cdot \nabla\varphi^{n+1} \, d\Omega = \int_\Omega \left(\frac{2\varepsilon}{\Delta t} - \sigma \right) \nabla\psi \cdot \nabla\varphi^n \, d\Omega, \tag{11}$$

$$\begin{aligned} &\int_\Omega \mu^{-1} \nabla \times \mathbf{w} \cdot \nabla \times \mathbf{A}^{n+1} \, d\Omega + \int_\Omega \frac{2\sigma}{\Delta t} \mathbf{w} \cdot \mathbf{A}^{n+1} \, d\Omega + \int_\Omega \left(\sigma + \frac{2\varepsilon}{\Delta t} \right) \mathbf{w} \cdot \nabla\varphi^{n+1} \, d\Omega \\ &= -\int_\Omega \mu^{-1} \nabla \times \mathbf{w} \cdot \nabla \times \mathbf{A}^n \, d\Omega + \int_\Omega \frac{2\sigma}{\Delta t} \mathbf{w} \cdot \mathbf{A}^n \, d\Omega - \int_\Omega \left(\sigma - \frac{2\varepsilon}{\Delta t} \right) \mathbf{w} \cdot \nabla\varphi^n \, d\Omega. \end{aligned} \tag{12}$$

A space-discrete variant is then obtained with the finite element method. More precisely, consider a triangulation of Ω, employ element-wise constant basis functions for the material coefficients, s first-order polynomial basis functions for the scalar EQS potential, and ν zeroth order Nédélec basis functions for the vectorial MQS potential to obtain the systems.

$$\mathbf{M}_{12}\boldsymbol{\phi}^{n+1} = \mathbf{b}_1^{n+1}, \qquad \mathbf{M}_{21}\mathbf{a}^{n+1} + \mathbf{M}_{22}\boldsymbol{\phi}^{n+1} = \mathbf{b}_2^{n+1}, \tag{13}$$

where $\mathbf{M}_{12} \in \mathbb{R}^{s\times s}$, $\mathbf{M}_{21} \in \mathbb{R}^{\nu\times\nu}$, $\mathbf{M}_{22} \in \mathbb{R}^{\nu\times s}$ are matrices that are associated with the left-hand-sides of Equations (11) and (12), while $\mathbf{b}_1 \in \mathbb{R}^s$ and $\mathbf{b}_2 \in \mathbb{R}^\nu$ are associated with the right-hand-sides of the same equations and the boundary conditions. These matrices are non-singular provided the partial gauging, the usage of Nédélec elements, continuity of the tangential component along interfaces, and boundary conditions. Since the first linear system of Equation (13) does not depend on the vectorial MQS potential, the scalar EQS potential $\boldsymbol{\phi}^{n+1}$ can be obtained first and can be substituted into the second linear system of Equation (13) for computing the vectorial MQS potential $\mathbf{a}^{n+1}$, that is,

$$\boldsymbol{\phi}^{n+1} = \mathbf{M}_{12}^{-1}\mathbf{b}_1^{n+1}, \qquad \mathbf{a}^{n+1} = \mathbf{M}_{21}^{-1}\mathbf{b}_2^{n+1} - \mathbf{M}_{21}^{-1}\mathbf{M}_{22}\mathbf{M}_{12}^{-1}\mathbf{b}_1^{n+1}. \tag{14}$$

Alternatively, a monolithic approach can be adopted, where the potentials $\boldsymbol{\phi}^{n+1}$, $\mathbf{a}^{n+1}$ are computed simultaneously by solving the compound linear system.

$$\begin{bmatrix} \mathbf{0} & \mathbf{M}_{12} \\ \mathbf{M}_{21} & \mathbf{M}_{22} \end{bmatrix} \begin{bmatrix} \mathbf{a}^{n+1} \\ \boldsymbol{\phi}^{n+1} \end{bmatrix} = \begin{bmatrix} \mathbf{b}_1^{n+1} \\ \mathbf{b}_2^{n+1} \end{bmatrix}. \tag{15}$$

Provided the potentials $\boldsymbol{\phi}^n$, $\mathbf{a}^n$ for all $n \in \{0, 1, ..., N\}$, the electric field intensity and the magnetic flux density are computed by

$$\mathbf{E}_h^n = -\nabla\varphi_h^n - \frac{\mathbf{A}_h^{n+1} - \mathbf{A}_h^{n-1}}{2\Delta t}, \qquad \mathbf{B}_h^n = \nabla\times\mathbf{A}_h^n, \tag{16}$$

where the subscript h is used for the associated finite element expansions.

Here, a two-step approach is also adopted for obtaining reference fields by solving the time-domain Maxwell equations, similarly to two-step frequency-domain schemes.[10,11] More precisely, as with the two-step EMQS method, initial-boundary value problem (6) is first solved, while the radiation term $\varepsilon\partial_{tt}\boldsymbol{A}$ is now taken into account and gauges the non-conductive regions by imposing the condition $\nabla\cdot\ \varepsilon\partial_{tt}\boldsymbol{A} = 0$. Thus, the equation that holds in $\Omega\times I$, see Equation (7), is replaced by

$$\nabla\times\mu^{-1}\nabla\times\mathbf{A} + \sigma\partial_t\mathbf{A} + \varepsilon\partial_{tt}\mathbf{A} = \mathbf{J}_{\mathrm{EQS}} \text{ in } \Omega\times I, \tag{17}$$

and hence, the associated variational problem reads as follows

$$\begin{aligned} &\text{find } \mathbf{A}\in H_0(\mathrm{curl},\Omega) \text{ such that } \int_\Omega \mu^{-1}\nabla\times\mathbf{w}\cdot\nabla\times\mathbf{A}\,\mathrm{d}\Omega + \int_\Omega \sigma\mathbf{w}\cdot\partial_t\mathbf{A}\,\mathrm{d}\Omega + \int_\Omega \varepsilon\mathbf{w}\cdot\partial_{tt}\mathbf{A}\,\mathrm{d}\Omega \\ &\qquad = \int_\Omega \mathbf{w}\cdot\mathbf{J}_{\mathrm{EQS}}\,\mathrm{d}\Omega \qquad \forall\mathbf{w}\in H_0(\mathrm{curl},\Omega). \end{aligned} \tag{18}$$

The time-discrete equation

$$
\begin{aligned}
&\int_\Omega \frac{1}{4\mu}\nabla\times\mathbf{w}\cdot\nabla\times\mathbf{A}^{n+1}\,\mathrm{d}\Omega+\int_\Omega\left(\frac{\sigma}{2\Delta t}+\frac{\varepsilon}{(\Delta t)^2}\right)\mathbf{w}\cdot\mathbf{A}^{n+1}\,\mathrm{d}\Omega\\
&\quad=-\int_\Omega \frac{1}{2\mu}\nabla\times\mathbf{w}\cdot\nabla\times\mathbf{A}^{n}\,\mathrm{d}\Omega+\int_\Omega\frac{2\varepsilon}{(\Delta t)^2}\mathbf{w}\cdot\mathbf{A}^{n}\,\mathrm{d}\Omega\\
&-\int_\Omega \frac{1}{4\mu}\nabla\times\mathbf{w}\cdot\nabla\times\mathbf{A}^{n-1}\,\mathrm{d}\Omega+\int_\Omega\left(\frac{\sigma}{2\Delta t}-\frac{\varepsilon}{(\Delta t)^2}\right)\mathbf{w}\cdot\mathbf{A}^{n-1}\,\mathrm{d}\Omega\\
&\quad+\int_\Omega\mathbf{w}\cdot\left(\frac{1}{4}\mathbf{J}_{\mathrm{EQS}}^{n+1}+\frac{1}{2}\mathbf{J}_{\mathrm{EQS}}^{n}+\frac{1}{4}\mathbf{J}_{\mathrm{EQS}}^{n-1}\right)\mathrm{d}\Omega
\end{aligned}
\tag{19}
$$

with $\mathbf{J}_{\mathrm{EQS}}^n=\varepsilon(\nabla\varphi^{n+1}-\nabla\varphi^{n-1})/(2\Delta t)+\sigma\nabla\varphi^n$ is obtained by employing a Newmark-Beta scheme[12,13] ($\gamma=1/2$, $\beta=1/4$).

The two-step EMQS approach in Equation (14) and the monolithic EMQS approach in Equation (15) are summarized in Algorithm 1 and Algorithm 2, respectively. In the following section, these two algorithms are numerically validated against the two-step Maxwell formulation.

3 | NUMERICAL EXPERIMENTS

The helical coil and the RLC circuit that are depicted in Figure 1 are used for verifying the schemes in a computational setting. The conductive material Ω_{C} and the dielectric material Ω_{D} are placed in a domain Ω, with $\Omega_{\mathrm{V}}=\Omega\setminus\overline{\Omega}_{\mathrm{C}}$ being void. A small artificial conductivity with a value of $2\varepsilon_0/\Delta t$ is introduced in the non-conductive regions to regularize the

Algorithm 1 **Two-step EMQS Scheme**

Require: Computational domain Ω, material functions ε, σ, μ, and boundary conditions
Ensure: Electromagnetic quasistatic field $\left(\mathbf{E}_h^n,\mathbf{B}_h^n\right)$
1: Initialization: $\mathbf{a}^{-1}$, $\mathbf{a}^0\leftarrow\mathbf{0}$, $\boldsymbol{\phi}^0\leftarrow\mathbf{0}$
2: **for** $n\leftarrow 0, 1, \ldots, N$ **do**
3: $\quad\boldsymbol{\phi}^{n+1}\leftarrow\mathbf{M}_{12}^{-1}\mathbf{b}_1^{n+1}$
4: end for.
5: **for** $n\leftarrow 0, 1, \ldots, N$ do
6: $\quad\mathbf{a}^{n+1}\leftarrow\mathbf{M}_{21}^{-1}\mathbf{b}_2^{n+1}-\mathbf{M}_{21}^{-1}\mathbf{M}_{22}\boldsymbol{\phi}^{n+1}$
7: $\quad\mathbf{E}_h^n\leftarrow-\nabla\varphi_h^n-\left(\mathbf{A}_h^{n+1}-\mathbf{A}_h^{n-1}\right)/(2\Delta t)$
8: $\quad\mathbf{B}_h^n\leftarrow\nabla\times\mathbf{A}_h^n$
9: end for

Algorithm 2 **Monolithic EMQS Scheme**

Require: Computational domain Ω, material functions ε, σ, μ, and boundary conditions.
Ensure: Electromagnetic quasistatic field $\left(\mathbf{E}_h^n,\mathbf{B}_h^n\right)$
1: Initialization: $\mathbf{a}^{-1}$, $\mathbf{a}^0\leftarrow\mathbf{0}$, $\boldsymbol{\phi}^0\leftarrow\mathbf{0}$
2: **for** $n\leftarrow 0, 1, \ldots, N$ **do**
3: $\quad$Solve problem (14) for $(\mathbf{a}^{n+1},\boldsymbol{\phi}^{n+1})$
4: $\quad\mathbf{E}_h^n\leftarrow-\nabla\varphi_h^n-\left(\mathbf{A}_h^{n+1}-\mathbf{A}_h^{n-1}\right)/(2\Delta t)$
5: $\quad\mathbf{B}_h^n\leftarrow\nabla\times\mathbf{A}_h^n$
6: end for

MQS problem. The material parameters of the devices are listed in Table 1. The boundary Γ_S supplies an excitation (5) whose frequency is $f = 10$ MHz and its maximum amplitude φ_{max} is equal to 12 V, while Γ_G is set to ground, and hence, $\varphi|\Gamma_G = 0$ for all $t \in [0, 3/f]$. The remaining part of the boundary is insulated. Provided that both the characteristic length $\ell_{HC} = 6$ cm of the helical coil and that of the RLC circuit, $\ell_{RLC} = 4$ cm, are smaller than half of the wavelength $\lambda \cong 30$ m that is associated with the operating frequency in void, the quasistatic assumption is expected to hold sufficiently well.

The time range is discretized with the trapezoidal rule for $\Delta t \in \{2.5, 1.25, 0.625\}$ ns and $N = 3/(f \cdot \Delta t)$, while the physical space is discretized with the finite element method, using first-order Lagrangian elements for the scalar EQS potential φ and lowest-order edge elements for the vectorial MQS potential $\boldsymbol{A}$. The number of degrees of freedom, the minimum mesh element size, and the average runtime per timestep are listed in Table 2. All algorithms are implemented using the finite element software FreeFEM[14] using PETSc[15] for parallelization and with MUMPS[16] as a solver. All simulations are run with 20 MPI processes.

The magnitude of the magnetic flux density and the electric field intensity for the helical coil and the RLC circuit obtained with the two-step EMQS scheme are depicted in Figure 2. For both devices the magnitude of the magnetic flux density is at its maximum within the coil and capacitive effects between the coil windings are visible in the plot of the magnitude of the electric field intensity. In the RLC circuit, the electric field intensity is strongest between the plates of the capacitor. A limitation of the discussed EMQS formulation is that induced displacement currents are neglected[17] and therefore, in combination with the employed artificial conductivity, a phase shift of the electric field can occur in between the capacitor plates.

The relative difference of the electric field intensity $\boldsymbol{E}$ and the magnetic flux density $\boldsymbol{B}$, defined as

$$\frac{\|\mathbf{F}_{I_1} - \mathbf{F}_{I_2}\|_{L^2(\Omega)}}{\|\mathbf{F}_{I_1}\|_{L^2(\Omega)}} \tag{20}$$

where $\boldsymbol{F} \in \{\boldsymbol{E}_h, \boldsymbol{B}_h\}$, $(I_1, I_2) \in \{(TS, M), (ML, M), (ML, TS)\}$, with the subscripts TS, ML, and M standing for the two-step, monolithic and full Maxwell schemes, respectively, and are depicted in Figures 3 and 4. In the same figures, observe that all differences are bounded from above, with reduced bounds for decreasing timesteps. The cause of the high-frequency oscillations is mainly related to the employed time-discretization. The relative differences between the fields that are obtained with the monolithic and the two-step EMQS algorithms for the RLC circuit are shown in Figure 5 and are less than 10^{-8} for the whole time-interval. Furthermore, the presented results are in agreement with the results previously presented, where the two-step EMQS scheme was compared to a two-step frequency-domain Maxwell solver.[8]

TABLE 1 Material parameters

Domain	Conductivity	Relative permittivity ε_r	Relative permeability μ_r
Ω_V	0 S/m ($\sigma_{artificial} = 2\varepsilon_0/\Delta t$)	1	1
Ω_C	$5.96 \cdot 10^7$ S/m	1	1
Ω_D	0 S/m ($\sigma_{artificial} = 2\varepsilon_0/\Delta t$)	2	1

TABLE 2 Number of Degrees of Freedom (dof), minimum cell size, and and average run time per timestep with the subscripts TS, ML, and M standing for the two-step, monolithic and full Maxwell schemes, respectively

	Lagrange elements	Nédélec elements	h_{min}	τ_{TS}	τ_{ML}	τ_M
Helical coil	40 045	285 265	$1.6 \cdot 10^{-4}$ m	2.6 s	2.6 s	4 s
RLC circuit	232 265	1 663 197	$1 \cdot 10^{-4}$ m	16.4 s	12.4 s	23.4 s

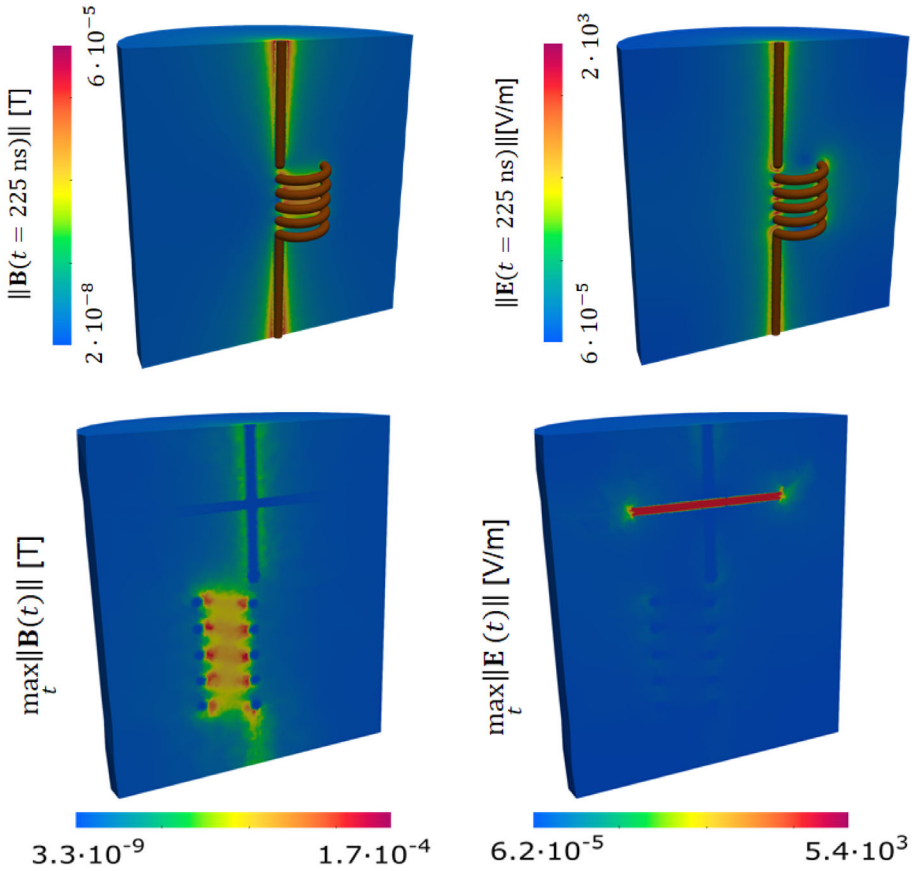

FIGURE 2 The magnitude of the magnetic flux density and the electric field intensity for the helical coil and the RLC circuit

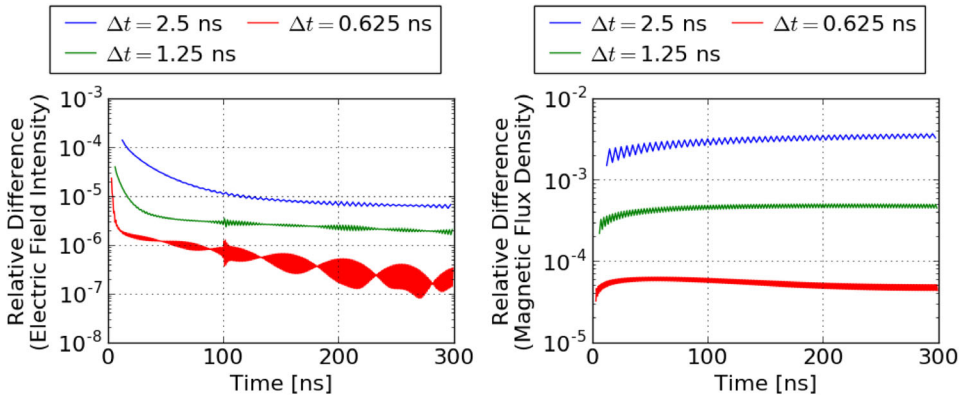

FIGURE 3 The relative difference of the electric field intensity and the magnetic flux density between two-step electromagnetic quasistatic scheme and the full Maxwell scheme for the helical coil

4 | CONCLUSIONS

Based on a previously developed two-step EMQS algorithm, we verified a monolithic EMQS scheme and proposed a two-step time-domain Maxwell algorithm. Here, it has been demonstrated that the fields that are obtained with the two-step EMQS algorithm, its monolithic variant, and the two-step Maxwell algorithm are in good agreement. Both two-step algorithms enable the usage of efficient solvers, due to the symmetry of the resulting linear systems, while the two-step EMQS algorithm has the benefit of requiring only first order derivative approximations with respect to time. All presented algorithms may require additional regularization in void, depending on the frequency of the excitation,

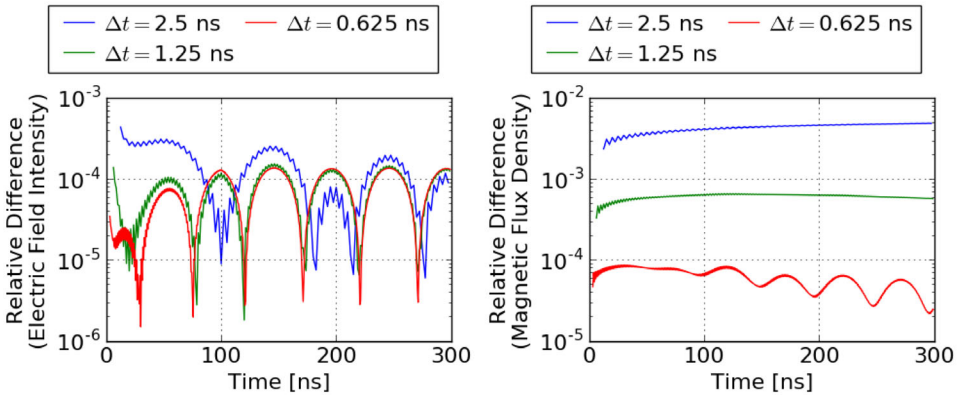

FIGURE 4 The relative difference of the electric field intensity and the magnetic flux density between two-step electromagnetic quasistatic scheme and the full Maxwell scheme for the RLC circuit

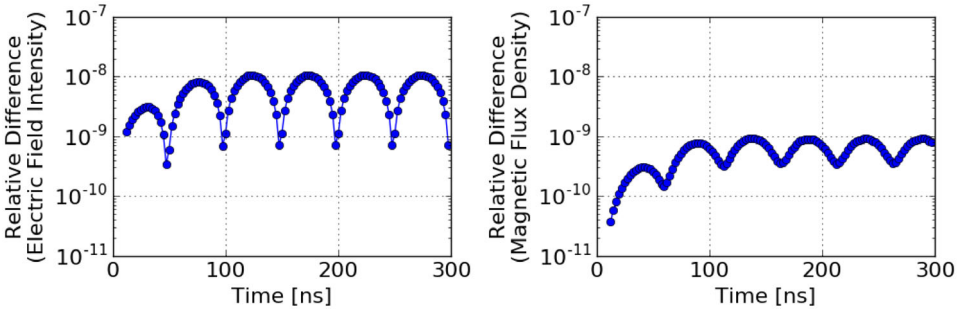

FIGURE 5 The relative difference of the electric field intensity and the magnetic flux density between monolithic and two-step electromagnetic quasistatic schemes for the RLC circuit for $\Delta t = 2.5$ ns

since the proposed electric field intensity computation requires a well-defined vectorial MQS potential throughout the computational domain.

ACKNOWLEDGMENT

This work was supported in parts by the Deutsche Forschungsgemeinschaft (DFG) under grants no. CL143/11-2 and CL143/18-1. Open Access funding enabled and organized by Projekt DEAL.

DATA AVAILABILITY STATEMENT

The data that support the findings of this study are available from the corresponding author upon reasonable request.

ORCID

Marvin-Lucas Henkel https://orcid.org/0000-0003-1440-923X
Fotios Kasolis https://orcid.org/0000-0003-1686-3946
Sebastian Schöps https://orcid.org/0000-0001-9150-0219
Markus Clemens https://orcid.org/0000-0002-1226-7840

REFERENCES

1. Darwin CLI. The dynamical motions of charged particles. *Lond Edinburgh Dublin Philos Mag J Sci*. 1920;39(233):537-551. doi:10.1080/14786440508636066
2. Raviart PA, Sonnendrücker E. Approximate models for the Maxwell equations. *J Comput Appl Math*. 1995;63(1–3):69-81. doi:10.1016/0377-0427(95)00058-5
3. Koch S, Weiland T. Different types of quasistationary formulations for time domain simulations: time domain quasistationary formulations. *Radio Sci*. 2011;46(5). doi:10.1029/2010RS004637

4. Koch S, Schneider H, Weiland T. A low-frequency approximation to the Maxwell equations simultaneously considering inductive and capacitive phenomena. *IEEE Trans Magn*. 2012;48(2):511-514. doi:10.1109/TMAG.2011.2173163
5. Zhao Y, Tang Z. A novel gauged potential formulation for 3-D electromagnetic field analysis including both inductive and capacitive effects. *IEEE Trans Magn*. 2019;55(6):1-5. doi:10.1109/TMAG.2019.2899288
6. Kaimori H, Mufune T, Kameari A. Novel application of coulomb gauge condition in electromagnetic FEM computations for Darwin approximation. *IEEE CEFC* 2020 Conference; 2020:87–92.
7. Bingler A, Bilicz S, Csornyei M, Badics Z. Thin-wire integral equation formulation with quasistatic Darwin approximation. *IEEE Trans Magn*. 2021;57(6):1-4. doi:10.1109/TMAG.2021.3064912
8. Clemens M, Kasolis F, Henkel ML, Kahne B, Gunther M. A two-step Darwin model time-domain formulation for quasi-static electromagnetic field calculations. *IEEE Trans Magn*. 2021;57(6):1-4. doi:10.1109/TMAG.2021.3057828
9. Jochum M, Farle O, Dyczij-Edlinger R. A new low-frequency stable potential formulation for the finite-element simulation of electromagnetic fields. *IEEE Trans Magn*. 2015;51(3):1-4. doi:10.1109/TMAG.2014.2360080
10. Ostrowski J, Hiptmair R. Frequency-stable full Maxwell in electro-quasistatic gauge. *SIAM J Sci Comput*. 2021;43(4):B1008-B1028. doi:10.1137/20M1356300
11. Henkel M, Kasolis F, Clemens M. A two-step Darwin model in frequency-domain for quasistatic electromagnetic field simulations. *21st ECMI Conference on Industrial and Applied Mathematics (ECMI 2021), Wuppertal, Germany, 13-15042021 Abstract*; 2021.
12. Newmark NM. A method of computation for structural dynamics. *J Eng Mech Div*. 1959;85(3):67-94. doi:10.1061/JMCEA3.0000098
13. Zienkiewicz OC. A new look at the Newmark, Houbolt and other time stepping formulas. A weighted residual approach. *Earthq Eng Struct Dyn*. 1977;5(4):413-418. doi:10.1002/eqe.4290050407
14. Hecht F. New development in FreeFem++. *J Numer Math*. 2012;20(3–4):251-265.
15. Balay S, Abhyankar S, Adams MF, et al. PETSc users manual. Tech. Rep. ANL-95/11 - Revision 3.15, Argonne National Laboratory; 2021.
16. Amestoy P, Duff IS, Koster J, L'Excellent JY. A fully asynchronous multifrontal solver using distributed dynamic scheduling. *SIAM J Matrix Anal Appl*. 2001;23(1):15-41.
17. Ostrowski J, Winkelmann C. Limitations of the two-step Darwin model in frequency domain. *IEEE Trans Magn*. 2022. doi:10.1109/TMAG.2022.3163611

How to cite this article: Henkel M-L, Kasolis F, Schöps S, Clemens M. A comparative study on electromagnetic quasistatic time-domain field calculations. *Int J Numer Model*. 2023;36(3):e3049. doi:10.1002/jnm.3049